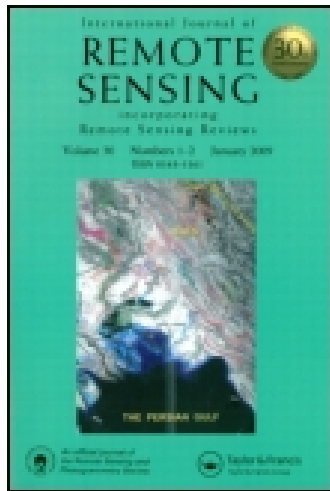


This article was downloaded by: [166.4.166.113]

On: 26 February 2015, At: 07:31

Publisher: Taylor & Francis

Informa Ltd Registered in England and Wales Registered Number: 1072954 Registered office: Mortimer House, 37-41 Mortimer Street, London W1T 3JH, UK



International Journal of Remote Sensing

Publication details, including instructions for authors and subscription information:

<http://www.tandfonline.com/loi/tres20>

Detection of burned areas from mega-fires using daily and historical MODIS surface reflectance

Rui Zhang^a, John J. Qu^b, Yongqiang Liu^c, Xianjun Hao^b, Chengquan Huang^a & Xiwu Zhan^d

^a Department of Geographical Sciences, University of Maryland, College Park, MD 20742, USA

^b The Global Environment and Natural Resources Institute, College of Science, George Mason University, Fairfax, VA 22030, USA

^c Center for Forest Disturbance Science, USDA Forest Service, Athens, GA 30602, USA

^d Center for Satellite Applications and Research (STAR), NESDIS/NOAA, College Park, MD 20740, USA

Published online: 23 Feb 2015.



[Click for updates](#)

To cite this article: Rui Zhang, John J. Qu, Yongqiang Liu, Xianjun Hao, Chengquan Huang & Xiwu Zhan (2015) Detection of burned areas from mega-fires using daily and historical MODIS surface reflectance, *International Journal of Remote Sensing*, 36:4, 1167-1187

To link to this article: <http://dx.doi.org/10.1080/01431161.2015.1007256>

PLEASE SCROLL DOWN FOR ARTICLE

Taylor & Francis makes every effort to ensure the accuracy of all the information (the "Content") contained in the publications on our platform. However, Taylor & Francis, our agents, and our licensors make no representations or warranties whatsoever as to the accuracy, completeness, or suitability for any purpose of the Content. Any opinions and views expressed in this publication are the opinions and views of the authors, and are not the views of or endorsed by Taylor & Francis. The accuracy of the Content should not be relied upon and should be independently verified with primary sources of information. Taylor and Francis shall not be liable for any losses, actions, claims, proceedings, demands, costs, expenses, damages, and other liabilities whatsoever or howsoever caused arising directly or indirectly in connection with, in relation to or arising out of the use of the Content.

This article may be used for research, teaching, and private study purposes. Any substantial or systematic reproduction, redistribution, reselling, loan, sub-licensing, systematic supply, or distribution in any form to anyone is expressly forbidden. Terms & Conditions of access and use can be found at <http://www.tandfonline.com/page/terms-and-conditions>

Detection of burned areas from mega-fires using daily and historical MODIS surface reflectance

Rui Zhang^{a*}, John J. Qu^b, Yongqiang Liu^c, Xianjun Hao^b, Chengquan Huang^a,
and Xiwu Zhan^d

^aDepartment of Geographical Sciences, University of Maryland, College Park, MD 20742, USA;

^bThe Global Environment and Natural Resources Institute, College of Science, George Mason University, Fairfax, VA 22030, USA; ^cCenter for Forest Disturbance Science, USDA Forest Service, Athens, GA 30602, USA; ^dCenter for Satellite Applications and Research (STAR), NESDIS/NOAA, College Park, MD 20740, USA

(Received 31 May 2014; accepted 30 November 2014)

The detection and mapping of burned areas from wildland fires is one of the most important approaches for evaluating the impacts of fire events. In this study, a novel burned area detection algorithm for rapid response applications using Moderate Resolution Imaging Spectroradiometer (MODIS) 500 m surface reflectance data was developed. Spectra from bands 5 and 6, the composite indices of the Normalized Burn Ratio, and the Normalized Difference Vegetation Index were employed as indicators to discover burned pixels. Historical statistical data were used to provide pre-fire baseline information. Differences in the current (post-fire) and historical (pre-fire) data were input into a support vector machine classifier, and the fire-affected pixels were detected and mapped by the support vector machine classification process. Compared with the existing MODIS level 3 monthly burned area product MCD45, the new algorithm is able to generate burned area maps on a daily basis when new data become available, which is more applicable to rapid response scenarios when major fire incidents occur. The algorithm was tested in three mega-fire cases that occurred in the continental USA. The experimental results were validated against the fire perimeter database generated by the Geospatial Multi-Agency Coordination Group and were compared with the MCD45 product. The validation results indicated that the algorithm was effective in detecting burned areas caused by mega-fires.

1. Introduction

Tens of thousands of wildfires occurred annually on an average between 1960 and 2012 in the USA burning over four million acres (16,187 km²) of forest and other ecosystems and threatening human lives and properties. In 2012, for example, 67,774 fire events were reported and consumed over nine million acres (36,422 km²) of wildland in total (NIFC 2013). The major damage was primarily caused by mega-fires that are often characterized as high intensity, high impact, and difficult to control; these events have recently increased (Liu, Goodrick, and Stanturf 2013). There is no quantitative definition for a 'mega-fire', but this term usually refers to extraordinary fire incidents in terms of their size, complexity, and resistance to control (Williams et al. 2005). For instance, the 2007 Georgia/Florida Okefenokee fires burned 0.6 million acres (2428.1 km²) during the entire burn period, which coincided with the worst drought in Georgia in a century.

*Corresponding author. Email: zhangrui@umd.edu

Together, these large fires represent <1% of all wildfires but cause most damage by accounting for 90% of the area burned and 80% of the suppression costs (Williams 2004).

The existing fire reporting system provides basic information on fires, that is, fire type, start and end dates, burned area, and other data. However, acquiring details of the spatial structure of daily fire processes are usually costly. Satellite remote sensing has emerged as an advanced technique for fire event identification. Satellites provide nearly global coverage of the Earth with spatial and temporal resolutions that vary from one platform to another. The Moderate Resolution Imaging Spectroradiometer (MODIS) instrument aboard NASA's Terra and Aqua platforms has improved fire monitoring capabilities, and several products that focus on fire events have been put into operational use, i.e. MOD14 – Thermal Anomalies – Fires and Biomass Burning (Justice et al. 2006) and MCD45 – MODIS burned area product (Roy et al. 2008, 2005). The satellite fire research community is currently working to secure necessary long-term fire observations from the next generation of operational satellite systems, such as the Joint Polar Satellite System (<http://www.jpss.noaa.gov>).

Current burned area detection algorithms that use remote sensors can be categorized into two groups: multitemporal change detection schemes and unitemporal spectral classification approaches. The methods of the first category usually compare pre- and post-fire data and detect spectral changes. The fire-affected areas are determined using preset criteria or thresholds via analyses of differences between two or multiple temporal data on sensitive variables. For instance, Barbosa, Grégoire, and Cardoso Pereira (1999) proposed an algorithm for extracting burned areas from the time series of Advanced Very High Resolution Radiometer (AVHRR) data at the continental scale, and the multitemporal and multispectral approaches were implemented based on spectral changes before and after a fire event. Roy et al. (2002, 2005, 2008) proposed change detection-based algorithms for fire-affected area mapping and compared the reflectance from a bi-directional reflectance model with the observed surface reflectance to locate burned areas using spectral changes. In addition, these algorithms were implemented with the MODIS MCD45 operational products. Kasischke et al. (1993) proposed an AVHRR-based multitemporal method to map boreal forest fires in Alaska in 1990. The forest fire boundaries were subtracted by comparing the late summer normalized difference vegetation index (NDVI) (Kriegler et al. 1969) composite image with an early summer scene.

Unitemporal spectral classification approaches commonly use knowledge of the spectral characteristics of burned vegetation, and the burned areas are identified by a series of spectral thresholds or a classification process. For example, Li et al. (2004) presented an empirical technique for detecting burned areas using MODIS level 1B top-of-atmosphere reflectance data. Several near-infrared (NIR) channels were used in the threshold process, which was based on the spectral analyses of characteristics of the pixels of burned areas. Petropoulos, Kontoes, and Keramitsoglou (2011) presented a burned area delineation method with unitemporal Landsat Thematic Mapper (TM) data using support vector machine (SVM) classification. The spectral differences between the burned and unburned pixels in the TM images were discovered implicitly in the SVM training process in the original spectral bands of TM, and the burned areas were mapped using an SVM classification process. Chuvieco, Martín, and Palacios (2002) proposed a burned area index to discriminate burned land in the red-NIR spectral domain, and the index was tested on Landsat TM and NOAA/AVHRR data. Pereira (1999) compared and assessed the performance of multiple vegetation indices in burned area detection and mapping, that is, NDVI, vegetation index 3 (VI3), global environmental monitoring index (GEMI), and a modified version of GEMI known as GEMI3; the author concluded that GEMI3

performed the best among the tested indices. Other burned area detection studies are available in the literature (Cahoon et al. 1994; Cao et al. 2009; Giglio et al. 2005; Libonati et al. 2010; Smith et al. 2007; Mitrakis et al. 2012). Comprehensive reviews of applications of remote-sensing techniques in assessing fire characteristics and post-fire effects can also be found (Emilio Chuvieco 1999; Lentile et al. 2006). Compared with unitemporal fire detection approaches, multitemporal methods involved additional information in decision-making, which may theoretically improve the performance of detections. Although the conclusion requires further verification, a comparative study on burned area detection from Landsat TM images and our preliminary experiments on MODIS data suggested that multitemporal algorithms might provide higher detection accuracies and more reliable performances than unitemporal methods (Kontoes et al. 2009).

This study builds upon research that integrating remote sensing-based burned area maps into wildfire caused smoke plume transport and process models (Heilman et al. 2014; Goodrick et al. 2013). In these studies, maps of major burns with high temporal resolutions are required as auxiliary variables in new models, and no available burned area products meet these requirements. This study also developed a general alternative mega-fire burned area detection algorithm using MODIS 500 m surface reflectance data for rapid response scenarios following major fire incidents at a regional scale. It provides higher temporal resolution (up to 1 day) than the MCD45 product (monthly available) with higher detection accuracy. Compared with the MOD14 Thermal Anomalies & Fire product (5-min/daily/8-day with 1 km resolution), the proposed algorithm provides higher spatial mapping resolution (500 m), and it focuses on mapping burned areas rather than locating active fire spots.

In the proposed algorithm, four predictors consisting of differences in the surface reflectances from MODIS bands 5 and 6, the normalized burn ratio (NBR) (Roy, Boschetti, and Trigg 2006), and the NDVI with the corresponding historical statistical average data were used as predictors (dB5, dB6, dNBR, and dNDVI) ('d' denotes difference). A burned/unburned pixel separation model was built using an SVM training process, and the burned pixels were determined by an SVM classification. This study differs from other previously proposed methods in which historical statistics are used as the baseline information, which offers the advantages of the high temporal resolution of unitemporal methods and the high detection accuracy of multitemporal change detection methods.

In this study, the proposed algorithm was trained and tested on six major mega-fire events that occurred in the continental USA. The detected burned area maps were validated against the Geospatial Multi-Agency Coordination Group (GeoMAC) fire perimeters database, and the detection accuracies of the new algorithm were compared with the accuracies of the MCD45 product.

2. Mega-fire events and data

2.1. Mega-fire events

Selected mega-fire events among the top 20 largest fires in recent years in the continental USA (refer to http://www.nifc.gov/fireInfo/fireInfo_stats_lgFires.html) were used in this study. Details on the fire cases are summarized in Table 1. The selection of the six used cases was decided by data quality, i.e. these fires had less persistent cloud cover than other top 20 cases according to visual inspections. The duration and location information for the fires were primarily retrieved from the websites of government agencies, for example, the

Table 1. Summary of the fire events including the fire name, starting and ending dates, total affected area in square kilometres, and the approximate locations in latitude and longitude.

Name	State	Duration	Total area (km ²)	Location
Murphy Complex	Idaho	16 July 2007–2 August 2007	2638.6	42° 17' N, 115° 8' W
Wallow	Arizona	29 May 2011–28 July 2011	2177.4	33° 48' N, 109° 19' W
Biscuit	Oregon	12 July 2002–15 July 2002	2023.7	42° 3' N, 123° 53' W
Big Turnaround Complex	Georgia	16 April 2007–18 June 2007	1565	30° 48' N, 82° 19' W
Milford Flat	Utah	6 July 2007–15 July 2007	1469.2	38° 39' N, 112° 46' W
Rock House	Texas	9 April 2011–7 May 2011	1272.5	31° 42' N, 100° 27' W

Bureau of Land Management (<http://www.blm.gov>) and the Earth Observatory of the National Aeronautics and Space Administration (<http://earthobservatory.nasa.gov/>). Portions of the information were obtained or confirmed from local media websites, which are not listed in Table 1.

2.2. Data

The daily 500 m surface reflectance data (MOD09GA) acquired by MODIS on board the Terra platform were the main data source for detecting burned areas in this study. The 8-day 500 m surface reflectance composite data (MOD09A1) from 2000 to 2013 with the same geolocation coverage, which was identified by the same MODIS Sinusoidal grid number, were also collected for calculating statistical averages. In addition to the surface reflectance data, the 250 m water–land mask data (MOD44W), which were primarily derived from the Shuttle Radar Topography Mission water body data, were also applied to exclude existing water pixels, such as rivers and lakes, from the burned area detection.

To validate the algorithm, a burned area perimeter database, which is updated daily and maintained by the GeoMAC (<http://wildfire.usgs.gov/geomac/index.shtml>), was used as the ground truth data. To ensure the accuracy of the validation, the acquisition dates of the satellite data and the coverage dates of the perimeter data for the same fire events were matched. The fire perimeter data are generated and updated daily based upon input from incident intelligence sources, GPS data, and infrared imagery from fixed wing and satellite platforms. A data quality check is performed before the perimeter data are loaded into the GeoMAC database (Walters, Schneider, and Guthrie 2011). Although the GeoMAC database is not an all-inclusive archive of fire incidents, the mapping accuracies of the perimeter data are generally satisfactory according to flight verifications on local scales (Thompson et al. 2013), which indicates that the GeoMAC data set is reliable and its accuracy is sufficient for the use as the ground truth data to validate a remote sensing-based burned area algorithm with a 500 m resolution. It is worth noting that the GeoMAC database only records relatively large burnings that are already known to exist, and it is not used to discover previously unreported burnings. In this study, the existence of the fire perimeters and the data quality for tested fire cases in the validations has been manually verified in the GeoMAC database. Because GeoMAC is not an all-inclusive database, it is unable to evaluate fire conditions for excluded cases, but it is able to assess burn scenes when the corresponding perimeter data are recorded in the GeoMAC database.

The obtained MODIS data in the sinusoidal grid were reprojected to the appropriate zones of the Universal Transverse Mercator projection with the world geodetic system 84 (WGS84) datum. All reprojection operations were set to a 500 m spatial resolution. The retrieved GeoMAC perimeter data in the ESRI shapefile format with the North American datum 83 were also reprojected to the WGS84 datum to match the satellite data accurately. Notably, cloud-contaminated pixels, which were identified by the quality assurance data set of MOD09GA data, were excluded prior to the classification. Only cloud-free pixels were used in the process of burned area detection.

In this study, three fire events were selected as training cases to generate the burned/unburned separation rules, and the remaining three fire events were used as test cases in the validation phase. The separation of the training and test cases was random, except for the Wallow case which was selected as a test case for detecting and tracking the development of burned areas in a time series. The isolation of training and test cases is to prevent the possible overfitting phenomenon that can occur in a pattern classifier. Detailed information on the fires in the experiments is listed in [Table 2](#).

In this article, the MODIS level 3 monthly product for mapping burned areas, known as MCD45, was used as a benchmark. The MCD45 algorithm detects changes in the MODIS band 5 data in daily time steps, and a multiple day statistical threshold z -score is used to separate the burned and unburned pixels. Additional details on the MCD45 algorithm can be found in (Roy et al. 2008).

3. Methodology

3.1. Spectral characteristics of the burned area

Many studies have already clearly characterized the spectral reflectance of burned areas observed by remote sensors and found that the major differences between burned and unburned vegetated areas are reduced reflectances in the NIR channels. For example, Li et al. (2004) provided an example of apparent reflectance spectra acquired with AVIRIS from NASA's ER-2 aircraft over Cuiaba, Brazil, on 25 August 1995. The burned and unburned vegetated area showed significant differences in the NIR channels, and

Table 2. Summary of the details of the experiments, including the name of the fire event, the affected ground ecosystems described by the land-cover classes, which were extracted from the MCD12 Land Cover product in the International Geosphere–Biosphere Programme category (Friedl et al. 2010), the acquisition date of the MODIS data, and the purpose of the case.

Name	Purpose	Land cover	Year and day of year
Murphy Complex	Training	Evergreen needleleaf forest, Woody savannahs, Grasslands	2007 209
Biscuit	Training	Evergreen needleleaf forest, Woody savannahs, Savannahs, Grasslands	2002 231, 238
Rock House	Training	Open shrublands, Grasslands	2011 107
Wallow	Test	Evergreen needleleaf forest, Open shrublands, Grasslands	2011 154, 157, 158, 160, 162, 163, 165, 167, 172
Big Turnaround Complex	Test	Evergreen needleleaf forest, Evergreen broadleaf forests, Mixed forests, Woody savannahs	2007 154
Milford Flat	Test	Open shrublands, Grasslands	2007 189

approximate reductions of 0.1–0.2 in the reflectance were observed (Li et al. 2004). For the MODIS sensors, the NIR band 5 (bandwidth centred on 1.24 μm), band 6 (1.64 μm), and band 7 (2.13 μm) are potential indicators for separating burned and unburned areas. The visible bands of MODIS (bands 1–4) were not directly used in this study because smoke caused by fires could be observed in these bands and could cover the burned-affected area. The phenomenon is mainly explained by the size of the smoke particles, which are usually larger than the wavelengths of the visible channels; as a result, significant scattering occurs in the visual bands (Li et al. 2004). However, bands 1 and 2 of the MODIS were indirectly used in the NDVI composite indices, and the scattering effects in these bands were mitigated by band ratio operations.

After comparing all collected surface reflectance data from post-fire or active-fire scenes, a single threshold that distinguishes burned from unburned areas is difficult to identify. The spectral reflectance of the burned areas in bands 5–7 varies considerably for different cases. A threshold can be easily built for a specific case with satisfactory performance, but that threshold usually performs poorly in another scene or another fire event. Other popular indices, for example, the NDVI and NBR which are used in many studies, also vary significantly in different scenes and cases. Figure 1 presents a comparison of several potential spectral signatures for burned areas among three fire cases.

Many factors contribute to the variation of the surface reflectance of the burned areas shown in Figure 1. For example, different vegetation types and the severity of fire events cause different levels of water content and chlorophyll loss and subsequently lead to variations in the reflective radiance received by the sensors. The variations in the surface reflectance among the cases indicate that the direct use of band reflectance or vegetation indices may be effective for specific cases of burned area detection, but it will be difficult to find stable and operable rules for general burned area detection algorithms.

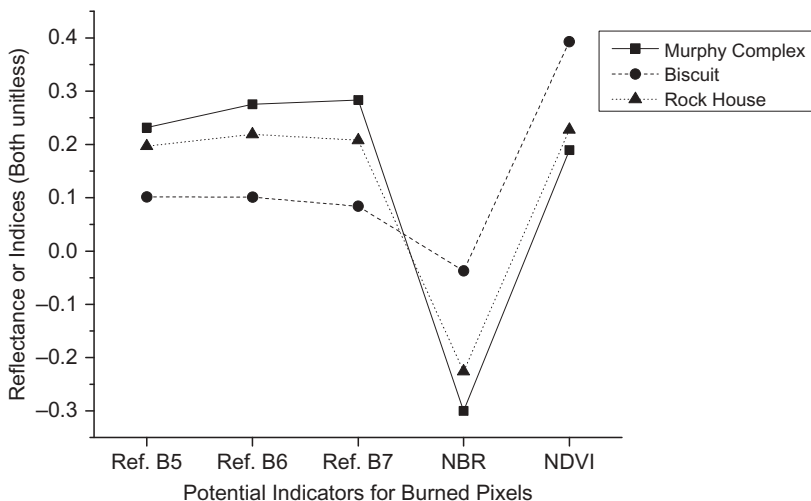


Figure 1. Spectral characteristics of burned areas in terms of extracted averages from regions of interest associated with three fire events in the USA. Ref, reflectance; NBR, normalized burned ratio; NDVI, normalized difference vegetation index. The values of each point in the figure represent the surface reflectance or index number and are all unit less.

3.2. Predictors

To alleviate the abovementioned instabilities of the reflectance characteristics in the burned areas, the proposed algorithm used spectral differences between post-fire and pre-fire reflectance data to increase the separability between the burned and unburned areas; the algorithm was based on the fact that reductions of reflectance in the NIR channels would be observed by remote sensors for fire-affected pixels. The commonly used solution for obtaining post-fire and pre-fire changes is to apply multiple year reflectance data in time series comparisons; fire-caused reflectance changes will be discovered by multitemporal data analyses. However, because the proposed algorithm is developed for rapid response for fire management systems, extensive data requirements, such as multiple day time series data input, are not operationally realistic. Therefore, in this study, historical statistical average data were used as the pre-fire baseline information instead of the time series data. Once the statistical data are generated, they can be stored in the system persistently and instantly applied to detect fire-affected areas when the daily surface reflectance is acquired. After comparisons and trials, four indicators of reflectance or indices were used to calculate the difference values, i.e. band 5 (centred on 1.24 μm), band 6 (centred on 1.64 μm), NBR calculated as the reflectance ratio (band 2 – band 7)/(band 2 + band 7), and the NDVI (band 2 – band 1)/(band 2 + band 1). After the difference calculation, dB5, dB6, dNBR, and dNDVI represented the final predictors used in this study. A line plot created from portions of the training samples comparing burned and unburned areas was presented to confirm that the applied difference calculation indeed increased the separability of these predictors, as shown in Figure 2. Details on the generation of the historical average are discussed in Section 5.

In Figure 2, the region of interest (ROI) of the burned/unburned areas was manually collected from the four-predictor data sets (dB5, dB6, dNBR, and dNDVI) and from the

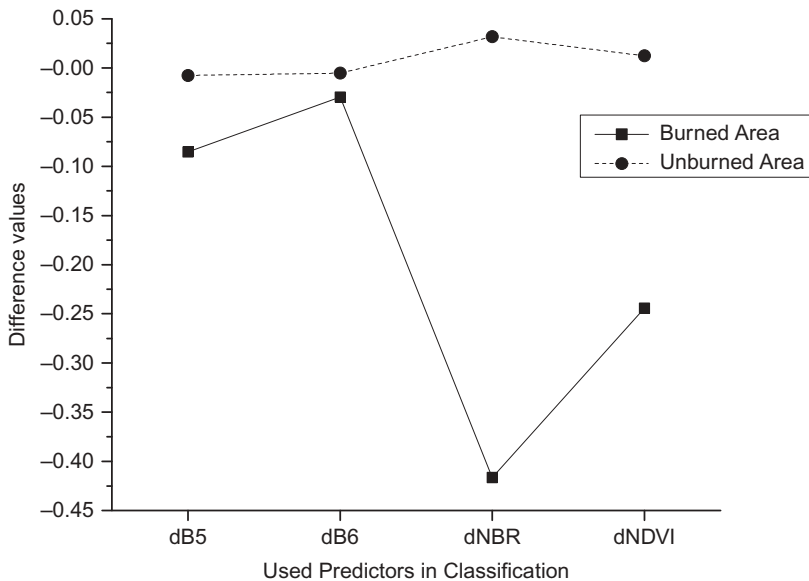


Figure 2. Comparisons between burned areas and unburned area for the four predictors. The values shown are averages calculated from training samples extracted from the regions of interest. In the average calculation, 9450 burned pixels were used, and 46,733 unburned pixels were used.

three fire cases selected for training. The burned areas could be visually distinguished from the difference data because of their significantly lower values compared with the surrounding unburned pixels. Unburned pixels were collected from the same images of fire cases, which included not only surrounding unburned vegetation pixels but also other non-water non-vegetated land-cover types. Figure 2 displays the average values of the four predictors for the burned and unburned samples, and the significant differences between the burned and unburned pixels can be observed. In general, the burned pixels exhibit negative values for all predictors due to reductions of the original indicators; the regular unburned pixels show dissimilar statistical results. Based on the quantitative analyses of the training samples used in Figure 2, ~75.6% of the burned class samples showed negative values for all four predictors, and only 4.72% of the samples of the unburned class in the training data showed negative values for all predictors. This result indicates that the general trend in the changes in the burn-affected areas is valid, but not every burned pixel follows the all-negative rule. Evidently, the separation of burned and unburned areas is more complicated than simple threshold partitioning. To capture the complexity of the patterns of differences between burned and unburned areas, rather than using intuitive thresholds, more powerful pattern recognition classification algorithms should be applied; thus more accurate separation rules would be generated through the training process.

3.3. Classifier

In this study, a classification algorithm known as an SVM was selected to separate the burned and unburned areas. As a promising pattern recognition technique, the SVM classifier has been extensively used in countless fields of research, including burned area detection using remote sensing (Cao et al. 2009; Petropoulos, Kontoes, and Keramitsoglou 2011). This algorithm locates an optimal discriminative boundary between binary classification problems using a relatively small training sample, and the kernel function provides the ability to generalize complicated classification problems with a small computational requirement. The SVM is designed to solve binary classification problems, but its function can be extended to include the computation of multiple classification problems by applying multiple SVMs simultaneously via a one-against-one or one-against-all schema. Because the required burned/unburned area separation is an obvious two-class problem, basic binary SVM classification was used in this study. Because the SVM classification techniques are generally well-known in the remote-sensing community and because many successful applications in remote sensing have been reported in the literature, the equations for the SVM are not included in this article. Detailed descriptions and explanations of the concepts behind the SVM can be found in Burges (1998), Cristianini and Shawe-Taylor (2000) and Vapnik (2000).

4. Validation

4.1. Validation design

Many SVM varieties and implementations are available for research, and the classic C -SVM implemented in Libsvm (Chang and Lin 2011) was selected here. A radial basis function (RBF) kernel was used in the experiments. Only two parameters, C and γ , need to be set before training. Parameter C is used to control the trade-off between

classification accuracy and tolerance error of the generated model. γ is the width of the RBF kernel, which controls the mapping from the original feature space into infinite dimensional space. A 10-fold cross validation process was applied to choose the optimal combination of the RBF parameters. The results showed that multiple parameter combinations yielded similar classification performance, including the combination of $C = 2000$ and $\gamma = 0.5$ used in this study. In addition, another commonly used kernel polynomial was also tested using a 10-fold cross validation, but no significant differences in classification accuracies were obtained compared with the RBF kernel. Hence, only the RBF kernel was used in the study.

In total, 56,183 pixels were used as training samples, including 9450 burned pixels and 46,733 unburned pixels. Burned and unburned pixels were identified by the GeoMAC data. All pixels in the burned/unburned ROIs were stacked into a binary training sample, and SVM training was conducted to obtain a binary classification model for separation rules. Water and cloud pixels were excluded using the MOD44W water–land mask and the quality assurance data set of the MOD09GA data, respectively. Except for water and clouds, all other land-cover types were treated as unburned in the training sample. As mentioned in ‘Section 2.2’, the training samples were completely independent of the test cases in the experiments as entirely different fire cases for training and testing were selected. The purpose was to avoid overfitting of the classifier because powerful classifiers, such as SVM, have the ability to generate a customized model for a specific problem, but lack generalization ability; thus, the performance of these models is usually poor in other cases.

4.2. Validation results

This section presents the validation results for three burned area detection cases. In Section 4.2.1, the mapped burned areas for the three cases tested with the new algorithm and the MCD45 product are shown, and the GeoMAC perimeter contours on the false colour reflectance data are also presented for visual comparison. Section 4.2.2 presents a time series comparison for the Wallow fire case. To demonstrate the significance of the progress of burning, only 3 day results with a 1 week interval are presented. Finally, the quantitative validations are presented in Section 4.2.3. Confusion matrices were used as an accuracy measurement for the proposed algorithm and the MCD45 product, and the converted GeoMAC perimeter vector data were taken as the ground truth image.

4.2.1. Three tested cases

In this subsection, the burned area detection results derived from the proposed algorithm, the MCD45 product, and GeoMAC database for the Wallow fire (2011), the Big Turnaround Complex fire (2007), and Milford Flat fire (2007) are presented in Figures 3, 4, and 5, respectively. Six major vegetation ecosystems, as listed in Table 2, were affected by these three wildland fires.

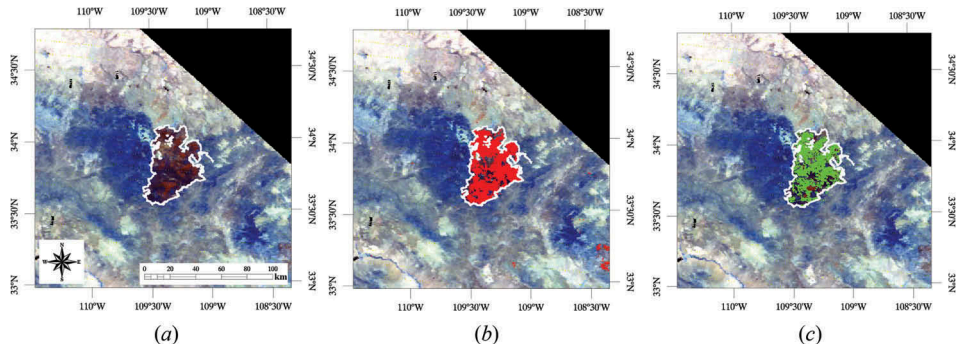


Figure 3. Wallow fire. Terra MODIS data acquired over Arizona, USA at 17:40 UTC, 11 June 2011: (a) false colour image (red: 2.13 μm , green: 1.64 μm , blue: 1.24 μm) with the GeoMAC burned area perimeter overlaid as a white contour; (b) burned area detected by the proposed algorithm (red); (c) MCD45 burned area product (green; the data are aggregated from day 149 to day 162).

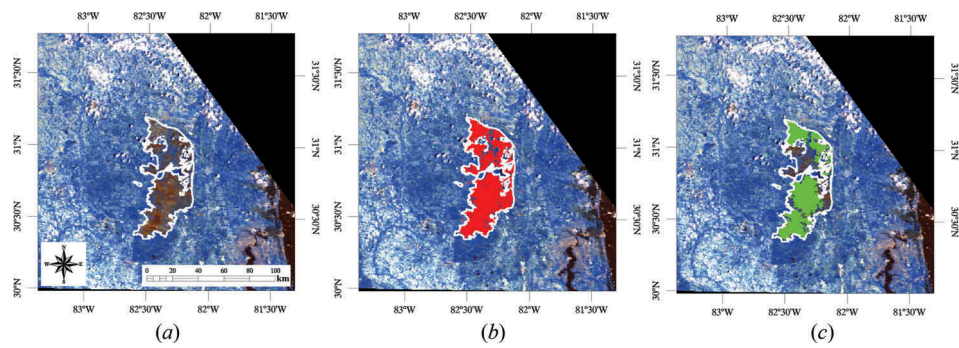


Figure 4. Big Turnaround Complex fire. Terra MODIS data acquired over Georgia, USA at 16:30 UTC, 3 June 2007: (a) false colour image (red: 2.13 μm , green: 1.64 μm , blue: 1.24 μm) with the GeoMAC burned area perimeter overlaid as a white contour; (b) burned area detected by the proposed algorithm (red); (c) MCD45 burned area product (green; the data are aggregated from day 106 to day 154).

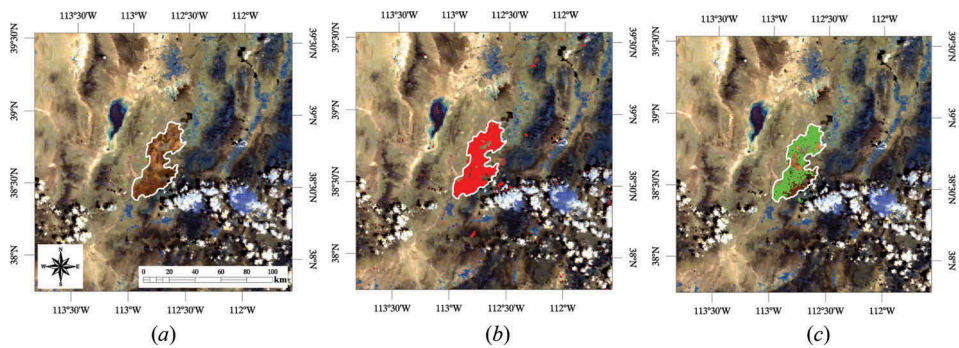


Figure 5. Milford Flat fire. Terra MODIS data acquired over Utah, USA at 17:05 UTC, 8 June 2007: (a) false colour image (red: 2.13 μm , green: 1.64 μm , blue: 1.24 μm) with the GeoMAC burned area perimeter overlaid as a white contour; (b) burned area detected by the proposed algorithm (red); (c) MCD45 burned area product (green; the data are aggregated from day 187 to day 189).

4.2.2. Time series of detected burned area for the Wallow fire

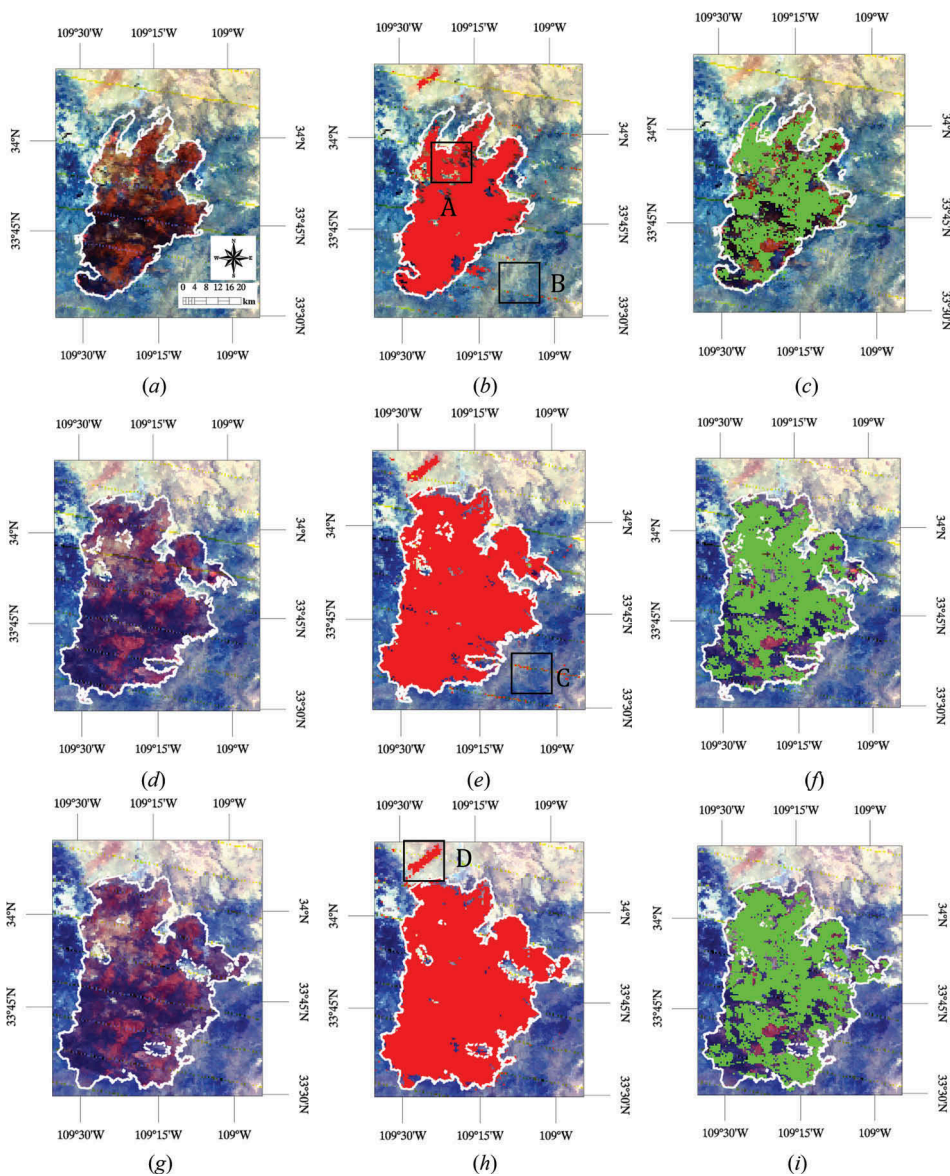


Figure 6. Zoomed in burned area development of the Wallow fire. All images are displayed in false colour (red: 2.13 μm , green: 1.64 μm , blue: 1.24 μm) overlaid with the perimeter vectors: (a) 7 June 2011 image; (b) burned area detected by the new algorithm; (c) burned area detected by the MCD45 product; (d) 14 June 2011 image; (e) burned area detected by the new algorithm; (f) burned area detected by the MCD45 product; (g) 21 June 2011 image; (h) burned area detected by the proposed algorithm; and (i) burned area detected by the MCD45 product.

4.2.3. Quantitative accuracy validations

To evaluate the accuracy of the burned area detection for the cases, 2×2 confusion matrices were used. The detection results obtained by the proposed algorithm and provided by the MCD45 product were evaluated with the GeoMAC fire perimeter data. Accuracy indicators were provided, including the kappa coefficient (κ), total accuracy, commission error of the burned pixels, and omission error of the burned pixels. The confusion matrices for all cases were calculated from $\sim 400 \times 400$ pixel windows.

It is worth noting that the GeoMAC fire perimeter vector data primarily stores the contour information for the fire-affected areas, and many details on the ground pixels inside the contours are ignored. In contrast, the detected burned areas are generated from a pixel-by-pixel classification process, and it is quite possible that pixels classified as unburned will appear inside the burned contour lines. Therefore, pixels classified as unburned surrounded by burned pixels or neglected unburned islands might generate multiple closed rings and isolated unburned pixels inside the fire perimeter regions in the detection maps. These rings and isolated unburned pixels do not necessarily mean that the algorithm omits these pixels as undetected. For example, in the square region A in [Figure 6\(b\)](#), the omitted pixels inside the burned areas might not represent omission errors based on visual inspections. The ground pixels with apparently high reflectance might not yet be burned or might be contaminated by active fire spots or other non-vegetative land cover. Therefore, the existence of these rings and pixels is reasonable, and the inconsistency of the two results may stem from the unique nature of each data set. To evaluate the accuracy using a consistent standard, the closed rings and isolated unburned pixels surrounded by burned areas in the detection maps were filled, i.e. reclassified as burned; this process maintained the consistency with the perimeter vector data. The same filling processes were applied to the results of the MCD45 products. This process was only applied for the accuracy measurement shown in [Tables 3 and 4](#), and [Figures 3–6](#) show the original detected mapping results without filling. This process is not a part of the operational burned area detection algorithm.

[Table 3](#) presents the confusion matrices for the proposed algorithm and the MCD45 product for the three mega-fire cases, which are described in [Section 4.2.1](#). A time series quantitative validation for the Wallow case was also conducted, and confusion matrices for the new algorithm and the MCD45 product are shown in [Table 4](#).

5. Discussions

5.1. Generation of historical average data

To obtain the difference values of the indicators, the first step was to generate the historical statistical average data that correspond to the daily surface reflectance. The statistical averages are presented as the simple mean value calculated as the direct summation divided by the number of years for each indicator of one pixel. As mentioned in [Section 2.2](#), the MOD09GA daily surface reflectance data were used for post-fire burned area detection, and the MOD09A1 8-day composite surface reflectance data were used to generate the historical average. The subtraction is performed between the post-fire daily data with the temporally closest 8-day pre-fire average data. The strategy is based on the assumption that over a short period of time, for example less than 8 days, the seasonal and inter-annual variations in the vegetative life cycle are not significant, and the obtained surface reflectance should be similar for a specific ROI, such as forest coverage areas. Cloud-affected pixels in the 8-day data are excluded in the average computation. Based on

Table 3. Accuracy comparisons of the burned area detected by the proposed algorithm and MCD45 product for the tested cases, as measured by confusion matrices. The GeoMAC perimeter data were taken as the ground truth data. The overall accuracies, commission errors, omission errors of burned areas, and κ coefficients are presented.

	Tested mega-fire cases								
	Wallow		Big Turnaround		Milford Flat				
	Burned ground truth (%)	Unburned ground truth (%)	Burned ground truth (%)	Unburned ground truth (%)	Burned ground truth (%)	Unburned ground truth (%)	Burned ground truth (%)	Unburned ground truth (%)	
The proposed algorithm	Burned identified	91.24	0.40	88.35	2.31	90.80	0.88		
	Unburned identified	8.76	99.60	11.65	97.69	9.20	99.12		
	Overall accuracy	99.18		96.95		98.85			
	Burned commission	7.65		23.44		22.17			
	Burned omission	8.76		11.65		9.20			
	Kappa coefficient (κ)	0.9136		0.8038		0.8322			
MCD45 product	Burned identified	79.18	0.13	51.46	0.04	69.38	0.07		
	Unburned identified	20.82	99.97	48.54	99.96	30.62	99.93		
	Overall accuracy	98.96		97.13		99.05			
	Burned commission	3.44		1.11		3.06			
	Burned omission	20.82		48.54		30.62			
	Kappa coefficient (κ)	0.8648		0.6635		0.8040			

Table 4. Accuracies of the burned area detected by the proposed algorithm for the Wallow case over time, as measured by confusion matrices. The GeoMAC perimeter data were taken as the ground truth data. The overall accuracies, commission errors, omission errors of burned areas, and κ coefficients are presented.

	Wallow case in time series						
	2011 158		2011 165		2011 172		
	Burned ground truth (%)	Unburned ground truth (%)	Burned ground truth (%)	Unburned ground truth (%)	Burned ground truth (%)	Unburned ground truth (%)	
The proposed algorithm	Burned identified	93.61	0.91	95.49	1.37	96.74	1.54
	Unburned identified	6.39	99.09	4.51	98.63	3.26	98.46
	Overall accuracy	98.88		98.45		98.35	
	Burned commission	20.09		19.42		19.05	
	Burned omission	6.39		4.51		3.26	
	Kappa coefficient (κ)	0.8564		0.8659		0.8726	
MCD45 product	Burned identified	69.89	0.10	70.62	0.17	76.98	0.14
	Unburned identified	30.11	99.90	29.38	99.83	23.02	99.86
	Overall accuracy	98.87		98.42		98.63	
	Burned commission	3.99		4.46		3.22	
	Burned omission	30.11		29.38		23.02	
	Kappa coefficient (κ)	0.8033		0.8040		0.8504	

the pre-fire assumption of the statistical data, the historical averages for operational use and for algorithm development use are different. In the operational phase, all of the 2000 to 2013 MOD09A1 8-day data will be used to calculate the statistical average. The historical average data will be calculated for each MODIS Sinusoidal grid tile (http://modis-land.gsfc.nasa.gov/MODLAND_grid.html) for every 8-day period. For instance, for the tile number h12v04 that covers portions of the northeast and mid-Atlantic regions of the USA, the average data for day 153, which covers observations from day 153 to day 160, will be generated using 2,000,153, 2,001,153, ..., 2,013,153 h12v04 8-day surface reflectance data. For each grid tile, 45 (365/8) 8-day data are calculated. Regarding the continental USA, for example, 15 tiles (number of MODIS sinusoidal tiles covering the continental USA) on 45 dates result in 675 historical average data sets. Depending on the geographical locations and vegetation types in the USA, the forest recovery time from major fire events varies, but it is usually much shorter than the total 14-year observational coverage provided by the MODIS data. For example, in the southeastern USA, re-grown vegetated areas become spectrally inseparable from unburned areas in only 4–6 years (Huang et al. 2010). Therefore, the 14-year data average, which represents normal circumstances, minimizes the possible impact of past fire incidents, and reduces other noises in the images, such as temporal data gaps caused by clouds. Because the generation of the operational historical average data is based on simple mathematical calculations using 8-day MODIS surface reflectance archive data and because no special steps are involved in the process, the creation of these historical data for general use is not difficult.

The strategy for generating historical averages for the algorithm development phase that is presented in this article is different from the approach above for operational use. Here, the average data were generated on demand for fire scenes using pre-fire years data only. For example, for the 2007 Big Turnaround Complex fire, to detect the burned area from the 154th daily data, the 2000–2006 day 153 MOD09A1 data, which was the closest pre-fire 8-day data, were collected; these data were used to calculate the historical pre-fire average. The major difference in the methods is that the historical data used in this article describes fire cases that occur in the past, and the average data for the operational use processes wildfires in the future. Both methods use pre-fire statistical average data as the baseline information for burned area detection. In this article, to ensure the quality of the historical average data, which are generated from temporally limited surface reflectances, the pre-fire data were manually checked to ensure that there are no other incidents that may also cause reductions of surface reflectances, such as previous fires, floods, and crop harvests.

The strategy of generating historical average data used in this article, which is referred as the ‘pre-fire method’, may introduce more noise and clouds in the generated average data, but it reveals the pre-fire conditions better than the operational generation strategy, which is referred to as the ‘all 14 years method’, because the speed of the disturbance–succession pathway for forests could vary significantly among tree species. Therefore, the ‘all 14 years method’ average data may not be very similar to the ‘pre-fire’ canopy conditions; as a result, different burned area detection results may be obtained. To evaluate the impact of historical data on the final burned area detection results, the two generation methods are compared in Section 5.3.

5.2. Comparisons with MCD45 products

Based on the visual comparisons of the burned area detection results presented in Figures 3–5, the geographical covers mapped with the proposed algorithm were more consistent

with the GeoMAC fire perimeter vector data compared with MCD45. Generally, the MCD45 data omitted a greater number of burned pixels than the proposed algorithm. The results could be explained by the conservative design of MCD45 for global implementation and validation (de Klerk, Wilson, and Steenkamp 2012).

In this study, κ was used as the primary indicator for evaluating the detection accuracy, instead of the total accuracy. κ is generally considered a more robust measure than a simple percentage calculation because κ takes into account the agreement that occurs by chance. From the accuracy comparisons for the three fire cases listed in Table 3, the newly proposed algorithm achieved higher κ values than the MCD45 algorithm (**0.9136** vs 0.8648, **0.8038** vs 0.6635, and **0.8322** vs 0.8040). The time series comparisons of the confusion matrices for the Wallow fire case in Table 4 also showed similar results (**0.8564** vs 0.8033, **0.8659** vs 0.8040, and **0.8726** vs 0.8504). Here, the bold values indicate higher κ or higher detection accuracies.

According to analyses of the confusion matrices and comparisons of the commission and omission errors of the burned areas, the new algorithm produced more committed errors and fewer omitted errors than the MCD45 product. For the three tested burned area cases, the proposed algorithm produced commission errors of 7.65%, 23.44%, and 22.17%. However, MCD45 produced commission errors of **3.44%**, **1.11%**, and **3.06%**. The omission errors for the proposed algorithm *versus* the MCD45 product for three cases were **8.76%** vs. 20.82%, **11.65%** vs. 48.54%, and **9.20%** vs. 30.62%. The results clearly indicate that the newly proposed algorithm is more aggressive in detecting burned areas. On the other hand, the MCD45 algorithm performs more conservatively in masking one pixel as burned.

The time series experiment for the Wallow fire confirmed the ability of the proposed algorithm to track the spatial development of the burned areas. The results from the MCD45 product were also included for comparison. Because MCD45 is a monthly product, the burn development of MCD45 was obtained by aggregately masking the burn dates that represent approximate the day of year of the burning from the beginning of the fire to the detection dates. According to the visual comparisons in Figure 6, the new algorithm captured the majority of the burned pixels development, and the consistencies between the mapping results and the GeoMAC perimeter vectors were high. MCD45 also discovered the burned areas during the fire progress, but more burned pixel omissions were observed. κ values obtained with the new algorithm and the MCD45 for the three observation dates were **0.8564** vs 0.8033, **0.8659** vs 0.8040, and **0.8726** vs 0.8504.

Based on examinations of the commission errors of the new algorithm, a portion of the committed errors were caused by residual errors from the applied cloud mask and contamination by cloud shadows, which can be observed in Figure 4(b). Sensor noise also introduced misclassified pixels in the burned area detection. For example, in Figure 6(b) region B and in Figure 6(e) region C, the isolated committed pixels shown in the zoomed view were caused by stripe noise in Terra band 5. Other commission errors of the proposed algorithm were caused by unexpected non-fire-related surface reflectance changes. In the zoomed view of region D in Figure 6(h), a patch of burned pixels was shown in the detected maps, but no perimeter polygon covered the same region. Visual inspection confirmed that this area had a lowered surface reflectance, while the historical statistics do not show the same reduction. This result indicates that other non-fire-related incidents occurred in this region. These commission errors suggest that the algorithm is unable to distinguish fires from other incidents that also cause a reduction of surface reflectance in the NIR bands, such as plant phenology, crop harvesting, and flooding. However, this drawback is common to other methods that use similar assumptions in the

signature of burned areas. Notably, the proposed algorithm is designed for rapid response systems for use by regional fire management authorities, and the demands of mapping burn area are only initiated by major fire incidents; hence, the approximate locations are already known from fire reporting systems, and the possibility of confusing of spectral changes in the NIR induced by fires with other causes is small.

The proposed algorithm omitted fewer burned pixels than the MCD45 product based on visual comparisons and quantitative analyses. According to the comparisons in [Figures 3\(b\) and \(c\)](#) and [Figures 5\(b\) and \(c\)](#), many burned pixels were not detected by the MCD45 algorithm. Inaccurate edges of the fire-affected areas were depicted by the MCD45, particularly for the Milford flat case shown in [Figure 5](#). The quantitative comparison in [Table 3](#) indicated that over 30% of the burned pixels were missing from the MCD45 results for this case. Comparisons for the Wallow time series also showed a similar trend for omission errors obtained by the proposed algorithm and the MCD45 product ([Figure 6](#) and [Table 4](#)). [Figures 6\(b\), \(e\), and \(h\)](#) showed considerably more accurate edge mapping results for the fire-affected areas than the results obtained for the MCD45 product in [Figures 6\(c\), \(f\), and \(i\)](#). The omission errors of 30.11%, 29.38%, and 23.02% obtained by the MCD45 product for three tested dates are significantly higher than the results obtained by the new algorithm, which yields omission errors of 6.39%, 4.51%, and 3.26%.

Based on the quantitative validations and visual inspections, the new algorithm outperformed the MCD45 algorithm in terms of the overall detection accuracy measured by κ for all tested cases, and the burned area mapping was more consistent with the GeoMAC perimeter data than the results of the MCD45 product. The new algorithm tends to detect burned pixels aggressively, and it omits fewer burned pixels than MCD45. The time series experiment confirmed that the newly proposed algorithm was able to detect and track the development of burned areas effectively.

5.3. Comparison between two historical data generation strategies

The 'pre-fire method' was used in generating historical average data in this article, and the detection results based on these 'pre-fire method' average data are presented in previous sections. In this subsection, the historical average data generated by the 'all 14 years method' were also tested for the three fire cases, and the accuracy comparisons measured by confusion matrices between the two strategies are presented in [Table 5](#). In the experiment, validation conditions were identical, except that the historical average data were generated by the 'pre-fire method' and the 'all 14 years method'.

Based on the confusion matrices presented in [Table 5](#), the two strategies yielded similar κ values for the Wallow fire case. The 'pre-fire method' achieved higher detection accuracies than the results from the 'all 14 years method' for the Big Turnaround and Milford Flat fire events. These inconsistent results indicated that >10 years of averages minimized the variations in the surface reflectances or indices caused by fires in some cases, but the inclusion of past fire incidents or other forest disturbances would affect the quality of the average data in some circumstances. Contributing factors may include different tree species, the different nature and duration of disturbance events, and the uncertainty of the data quality, such as the presence of noise and cloud contamination in the surface reflectance. Although the detection accuracy using the 'all 14 years method' average data decreased in two cases, the obtained κ values were higher than those achieved by the MCD45 products for all three tested cases; thus, the proposed algorithm outperformed the MCD45 algorithm regardless of the averaging strategy employed.

Table 5. Accuracy comparisons of the burned area detection using 'pre-fire' average data and 'all 14 years' average data for the tested cases, as measured by confusion matrices. The GeoMAC perimeter data were taken as the ground truth data. The overall accuracies, commission errors, omission errors of burned areas, and kappa coefficients (κ) are presented.

	Tested mega-fire cases								
	Wallow		Big Turnaround		Milford Flat				
	Burned ground truth (%)	Unburned ground truth (%)	Burned ground truth (%)	Unburned ground truth (%)	Burned ground truth (%)	Unburned ground truth (%)	Burned ground truth (%)	Unburned ground truth (%)	
'Pre-fire' average	Burned identified	91.24	0.40	88.35	2.31	90.80	0.88		
	Unburned identified	8.76	99.60	11.65	97.69	9.20	99.12		
	Overall accuracy	99.18		96.95		98.85			
	Burned commission	7.65		23.44		22.17			
	Burned omission	8.76		11.65		9.20			
	Kappa coefficient (κ)	0.9136		0.8038		0.8322			
'All 14 years' average	Burned identified	91.17	0.33	85.28	3.62	91.58	1.06		
	Unburned identified	8.83	99.67	14.72	96.38	8.42	98.94		
	Overall accuracy	99.24		95.51		98.70			
	Burned commission	6.42		33.18		25.32			
	Burned omission	8.83		14.72		8.42			
	Kappa coefficient (κ)	0.9196		0.7250		0.8161			

6. Conclusions

This article proposed a new burned area detection algorithm based on MODIS 500 m surface reflectance and historical statistics for time-sensitive applications. Differences between the surface reflectance or indices and statistical averages (dB5, dB6, dNBR, and dNDVI) were employed as predictors. Separation of the burned from unburned areas was achieved using the SVM classifier. The trend of reduced reflectances or indices in the burned areas was captured by the SVM training process, and separation rules were expressed in the SVM model implicitly. The newly proposed algorithm was validated against the GeoMAC fire perimeter data set using three fire cases. The results indicated that the proposed algorithm is effective and stable in detecting fire-affected areas from MODIS surface reflectance data. Comparisons with the MCD45 product data suggested that the new algorithm outperforms the MCD45 algorithm in terms of detection accuracy.

The proposed algorithm requires the visible and NIR bands of remote-sensing data for detecting burned areas; therefore, this method shares the disadvantages observed in many optical remote-sensing techniques. For example, a clear ground view is always critical for any Earth observation-related applications, but the availability of remote-sensing data with clear views over fire scenes is not always guaranteed. Other noise caused by sensors, cloud masks, and cloud shadows will also introduce commission and omission errors in burned pixel detection.

Benefiting from the high temporal resolution and minimal data input, the algorithm could be used as an alternative approach in rapid response systems for fire management authorities, such as the USA forest service. However, comprehensive validations should be conducted prior to deployment in operational environments. In addition, the currently proposed burned area detection algorithm was developed based only on data acquired over the continental USA because only USA data are included in the GeoMAC validation database; therefore, more training samples obtained from other regions of the world are required to build a more general detection model for applications in other regional fire management authorities.

Acknowledgements

The authors would like to thank the reviewers for their valuable comments. The manuscript contents are solely the opinions of the authors and do not constitute a statement of policy, decision, or position on behalf of US Department of Agriculture, National Oceanic and Atmospheric Administration, or the US Government.

Disclosure statement

No potential conflict of interest was reported by the authors.

Funding

This study was supported by the USA Joint Fire Science Program [Agreement No. JFSP 11172].

References

- Barbosa, P. M., J.-M. Grégoire, and J. M. Cardoso Pereira. 1999. "An Algorithm for Extracting Burned Areas from Time Series of AVHRR GAC Data Applied at a Continental Scale." *Remote Sensing of Environment* 69 (3): 253–263. doi:10.1016/S0034-4257(99)00026-7.
- Burges, C. J. C. 1998. "A Tutorial on Support Vector Machines for Pattern Recognition." *Data Mining and Knowledge Discovery* 2 (2): 121–167. doi:10.1023/A:1009715923555.

- Cahoon, D. R., B. J. Stocks, J. S. Levine, W. R. Cofer, and J. M. Pierson. 1994. "Satellite Analysis of the Severe 1987 Forest Fires in Northern China and Southeastern Siberia." *Journal of Geophysical Research* 99 (D9): 18627. doi:10.1029/94JD01024.
- Cao, X., J. Chen, B. Matsushita, H. Imura, and L. Wang. 2009. "An Automatic Method for Burn Scar Mapping Using Support Vector Machines." *International Journal of Remote Sensing* 30 (3): 577–594. doi:10.1080/01431160802220219.
- Chang, C.-C., and C.-J. Lin. 2011. "LIBSVM: A Library for Support Vector Machines." *ACM Transactions on Intelligent Systems and Technology* 2 (3): 1–27. doi:10.1145/1961189.1961199.
- Chuvieco, E., M. P. Martín, and A. Palacios. 2002. "Assessment of Different Spectral Indices in the Red-near-Infrared Spectral Domain for Burned Land Discrimination." *International Journal of Remote Sensing* 23 (23): 5103–5110. doi:10.1080/01431160210153129.
- Chuvieco, E. 1999. *Remote Sensing of Large Wildfires in the European Mediterranean Basin*. Berlin: Springer.
- Cristianini, N., and S.-T. John. 2000. *An Introduction to Support Vector Machines and Other Kernel-Based Learning Methods*. Cambridge: Cambridge University Press.
- de Klerk, H. M., A. M. Wilson, and K. Steenkamp. 2012. "Evaluation of Satellite-Derived Burned Area Products for the Fynbos, a Mediterranean Shrubland." *International Journal of Wildland Fire* 21 (1): 36. doi:10.1071/WF11002.
- Friedl, M. A., D. Sulla-Menashe, B. Tan, A. Schneider, N. Ramankutty, A. Sibley, and X. Huang. 2010. "MODIS Collection 5 Global Land Cover: Algorithm Refinements and Characterization of New Datasets." *Remote Sensing of Environment* 114 (1): 168–182. doi:10.1016/j.rse.2009.08.016.
- Giglio, L., G. R. Van Der Werf, J. T. Randerson, G. J. Collatz, and P. Kasibhatla. 2005. "Global Estimation of Burned Area Using MODIS Active Fire Observations." *Atmospheric Chemistry and Physics Discussions* 5 (6): 11091–11141. doi:10.5194/acpd-5-11091-2005.
- Goodrick, S. L., G. L. Achtemeier, N. K. Larkin, Y. Liu, and T. M. Strand. 2013. "Modelling Smoke Transport from Wildland Fires: A Review." *International Journal of Wildland Fire* 22 (1): 83. doi:10.1071/WF11116.
- Heilman, W. E., Y. Liu, S. Urbanski, V. Kovalev, and R. Mickler. 2014. "Wildland Fire Emissions, Carbon, and Climate: Plume Rise, Atmospheric Transport, and Chemistry Processes." *Forest Ecology and Management* 317 (Apr): 70–79. doi:10.1016/j.foreco.2013.02.001.
- Huang, C., S. N. Goward, J. G. Masek, N. Thomas, Z. Zhu, and J. E. Vogelmann. 2010. "An Automated Approach for Reconstructing Recent Forest Disturbance History Using Dense Landsat Time Series Stacks." *Remote Sensing of Environment* 114 (1): 183–198. doi:10.1016/j.rse.2009.08.017.
- Justice, C., L. Giglio, L. Boschetti, D. Roy, I. Csiszar, J. Morisette, and Y. Kaufman. 2006. *MODIS Fire Products: Algorithm Technical Background Document*. Greenbelt, MD: Goddard Space Flight Center, National Aeronautics and Space Administration.
- Kasischke, E. S., H. F. Nancy, P. H. French, N. L. Christensen, S. L. Ustin, and D. Barry. 1993. "Monitoring of Wildfires in Boreal Forests Using Large Area AVHRR NDVI Composite Image Data." *Remote Sensing of Environment* 45 (1): 61–71. doi:10.1016/0034-4257(93)90082-9.
- Kontoes, C. C., H. Poilvé, G. Florsch, I. Keramitsoglou, and S. Paralikidis. 2009. "A Comparative Analysis of a Fixed Thresholding vs. a Classification Tree Approach for Operational Burn Scar Detection and Mapping." *International Journal of Applied Earth Observation and Geoinformation* 11 (5): 299–316. doi:10.1016/j.jag.2009.04.001.
- Kriegler, F. J., W. A. Malila, R. F. Nalepka, and W. Richardson. 1969. "Preprocessing Transformations and Their Effects on Multispectral Recognition." *Remote Sensing of Environment, VI* 1: 97–131.
- Lentile, L. B., Z. A. Holden, A. M. S. Smith, M. J. Falkowski, A. T. Hudak, P. M. Morgan, S. A. Lewis, P. E. Gessler, and N. C. Benson. 2006. "Remote Sensing Techniques to Assess Active Fire Characteristics and Post-Fire Effects." *International Journal of Wildland Fire* 15 (3): 319. doi:10.1071/WF05097.
- Li, R.-R., Y. J. Kaufman, W. M. Hao, J. M. Salmon, and B.-C. Gao. 2004. "A Technique for Detecting Burn Scars Using MODIS Data." *IEEE Transactions on Geoscience and Remote Sensing* 42 (6): 1300–1308. doi:10.1109/TGRS.2004.826801.
- Libonati, R., C. C. DaCamara, J. M. C. Pereira, and L. F. Peres. 2010. "Retrieving Middle-Infrared Reflectance for Burned Area Mapping in Tropical Environments Using MODIS." *Remote Sensing of Environment* 114 (4): 831–843. doi:10.1016/j.rse.2009.11.018.

- Liu, Y., S. L. Goodrick, and J. A. Stanturf. 2013. "Future U.S. Wildfire Potential Trends Projected Using a Dynamically Downscaled Climate Change Scenario." *Forest Ecology and Management* 294 (Apr): 120–135. doi:10.1016/j.foreco.2012.06.049.
- Mitrakis, N. E., G. Mallinis, N. Koutsias, and J. B. Theocharis. 2012. "Burned Area Mapping in Mediterranean Environment Using Medium-Resolution Multi-Spectral Data and a Neuro-Fuzzy Classifier." *International Journal of Image and Data Fusion* 3 (4): 299–318. doi:10.1080/19479832.2011.635604.
- NIFC. 2013. *Total Wildland Fires and Acres (1960-2012)*. http://www.nifc.gov/fireInfo/fireInfo_stats_totalFires.html.
- Pereira, J. M. C. 1999. "A Comparative Evaluation of NOAA/AVHRR Vegetation Indexes for Burned Surface Detection and Mapping." *IEEE Transactions on Geoscience and Remote Sensing* 37 (1): 217–226. doi:10.1109/36.739156.
- Petropoulos, G. P., C. Kontoes, and I. Keramitsoglou. 2011. "Burnt Area Delineation from a Uni-Temporal Perspective Based on Landsat TM Imagery Classification Using Support Vector Machines." *International Journal of Applied Earth Observation and Geoinformation* 13 (1): 70–80. doi:10.1016/j.jag.2010.06.008.
- Roy, D. P., L. Boschetti, C. O. Justice, and J. Ju. 2008. "The Collection 5 MODIS Burned Area Product — Global Evaluation by Comparison with the MODIS Active Fire Product." *Remote Sensing of Environment* 112 (9): 3690–3707. doi:10.1016/j.rse.2008.05.013.
- Roy, D. P., L. Boschetti, and S. N. Trigg. 2006. "Remote Sensing of Fire Severity: Assessing the Performance of the Normalized Burn Ratio." *IEEE Geoscience and Remote Sensing Letters* 3 (1): 112–116. doi:10.1109/LGRS.2005.858485.
- Roy, D. P., Y. Jin, P. E. Lewis, and C. O. Justice. 2005. "Prototyping a Global Algorithm for Systematic Fire-Affected Area Mapping Using MODIS Time Series Data." *Remote Sensing of Environment* 97 (2): 137–162. doi:10.1016/j.rse.2005.04.007.
- Roy, D. P., P. E. Lewis, and C. O. Justice. 2002. "Burned Area Mapping Using Multi-Temporal Moderate Spatial Resolution Data—A Bi-Directional Reflectance Model-Based Expectation Approach." *Remote Sensing of Environment* 83 (1–2): 263–286. doi:10.1016/S0034-4257(02)00077-9.
- Smith, A. M. S., N. A. Drake, M. J. Wooster, A. T. Hudak, Z. A. Holden, and C. J. Gibbons. 2007. "Production of Landsat ETM+ Reference Imagery of Burned Areas within Southern African Savannahs: Comparison of Methods and Application to MODIS." *International Journal of Remote Sensing* 28 (12): 2753–2775. doi:10.1080/01431160600954704.
- Thompson, M. P., D. E. Calkin, J. Herynk, C. W. McHugh, and K. C. Short. 2013. "Airtankers and Wildfire Management in the US Forest Service: Examining Data Availability and Exploring Usage and Cost Trends." *International Journal of Wildland Fire* 22 (2): 223. doi:10.1071/WF11041.
- Vapnik, V. 2000. *The Nature of Statistical Learning Theory*. New York: Springer.
- Walters, S. P., N. J. Schneider, and J. D. Guthrie. 2011. *Geospatial Multi-Agency Coordination (GeoMAC) Wildland Fire Perimeters, 2008*, DS612. Reston, VA: US Geological Survey.
- Williams, J. 2004. "Managing Fire-Dependent Ecosystems: We Need a Public Lands Policy Debate." *Fire Management Today* 64 (2): 6–11.
- Williams, J., L. Hamilton, R. Mann, M. Rounsaville, H. Leonard, O. Daniels, and D. Bunnell. 2005. *The Mega-Fire Phenomenon: Toward a More Effective Management Model*. Washington, DC: Brookings Institution.